Revealing superstructure ordering in $Co_{1+x}MnSb$ Heusler alloys and its effect on structural, magnetic, and electronic properties

Madhusmita Baral [1,2,*] Velega Srihari [3] Ashok Bhakar [1,2] M. K. Chattopadhyay,[2,4] Pragya Tiwari,[1]
Aparna Chakrabarti,[2,5] and Tapas Ganguli[1,2]

[1]*Synchrotrons Utilization Section, Raja Ramanna Centre for Advanced Technology, Indore 452 013, India*
[2]*Homi Bhabha National Institute, Training School Complex, Anushakti Nagar, Mumbai 400 094, India*
[3]*High Pressure and Synchrotron Radiation Physics Division, Bhabha Atomic Research Centre, Mumbai 400 085, India*
[4]*Free Electron Laser Utilization Laboratory, Raja Ramanna Centre for Advanced Technology, Indore 452 013, India*
[5]*Theory and Simulations Laboratory, Raja Ramanna Centre for Advanced Technology, Indore 452 013, India*

We have performed a combined experimental and theoretical study of the $Co_{1+x}MnSb$ system to understand the progressive evolution of the crystal structure and physical properties as a function of Co content. We find that all the arc-melted polycrystalline samples show superstructure ordering similar to CoMnSb. In the CoMnSb superstructure with Fm-$3m$ symmetry, one set of the $32f$ sites is filled with Co atoms while the other set is vacant. With increasing Co content, although the vacant set of $32f$ sites gets progressively filled with the Co atoms, some of the Co atoms segregate out of the main phase into the grain boundaries. The maximum Co that enters in the $Co_{1+x}MnSb$ phase is $x = \sim0.45$. Thus, we find that the theoretically predicted Co_2MnSb in $L2_1$ phase does not stabilize. All the samples are ferromagnetic above room temperature and the trend in the measured magnetic moments with increasing x, agrees reasonably well with the density-functional theory calculations done using the structural and compositional parameters obtained from the Rietveld refinement of the synchrotron x-ray diffraction patterns. However, the electronic structure indicates that in spite of the large magnetic moment, none of the alloys are half metallic. Finally, we find that a minor deviation from stoichiometry in CoMnSb, i.e., excess of Co and Sb as compared to Mn, is accommodated in the set of vacant $32f$ sites of the superstructure. This explains the increase in the lattice parameter and the saturation magnetization, as compared to the calculated stoichiometric CoMnSb superstructure. Calculations also predict that this minor deviation from stoichiometry destroys the half metallicity in the CoMnSb superstructure.

I. INTRODUCTION

Half-metallic (HM) materials, showing metallic character in one of the spin channels and semiconducting band gap at the Fermi level (E_f) in the other spin channel, have been of immense interest to researchers for the last several decades because of their potential in spintronics [1–4]. Since the prediction of the first half metal, NiMnSb by de Groot *et al.* [1], the search for half metals in the family of half and full Heusler alloys remains an important topic of research. This is mainly because of their high Curie temperature (T_C) and structural compatibility with many technologically important conventional semiconductors, both of which are essential parameters for device fabrication [4–10]. The half-Heusler alloys with chemical formula ABC generally crystallize in the cubic $C1_b$ structure (F-$43m$ space group), where A and B are transition-metal atoms and C is an sp block element. The conventional full-Heusler alloy A_2BC, which consists of four interpenetrating fcc sublattices, crystallizes in the $L2_1$ structure (Fm-$3m$ space group). The crystal structure of ABC can be derived from the A_2BC, where one of the two equivalent A sites is

empty. Any intermediate composition, $A_{1+x}BC$ ($0 \leqslant x \leqslant 1$) is formed in the incompletely filled $L2_1$ structure, with partial occupancy of the atoms in the vacant A site.

Among the family of Heusler alloys, Co-Mn-Sb is an interesting system as both CoMnSb in $C1_b$ structure [shown in Fig. 1(a)] [8,10–12] and Co_2MnSb in $L2_1$ structure [shown in Fig. 1(b)] [12–16] were theoretically predicted to be HM ferromagnets with calculated total spin magnetic moments of 3 and 6 μ_B per formula unit (f.u.), respectively. The E_f is situated at the bottom of the HM gap in the minority spin states of CoMnSb, but shifts to the top of the HM gap in Co_2MnSb. However, the experimentally observed crystal structure and magnetic moment of these materials were reported [17–23] to be significantly different from those obtained from the calculations [8,10–16]. While CoMnSb forms in the superstructure phase (Fm-$3m$ space group) with an enhanced magnetic moment and metallic nature [17–22], Co_2MnSb is found in the incompletely filled $L2_1$ structure with actual composition different from the stoichiometry and has a reduced magnetic moment [23]. Moreover, the structural and physical properties of the intermediate compositions also remain unexplored so far. Thus, a combined in-depth experimental and theoretical study of CoMnSb, Co_2MnSb, and the intermediate compositions of $Co_{1+x}MnSb$ is required for understanding

---

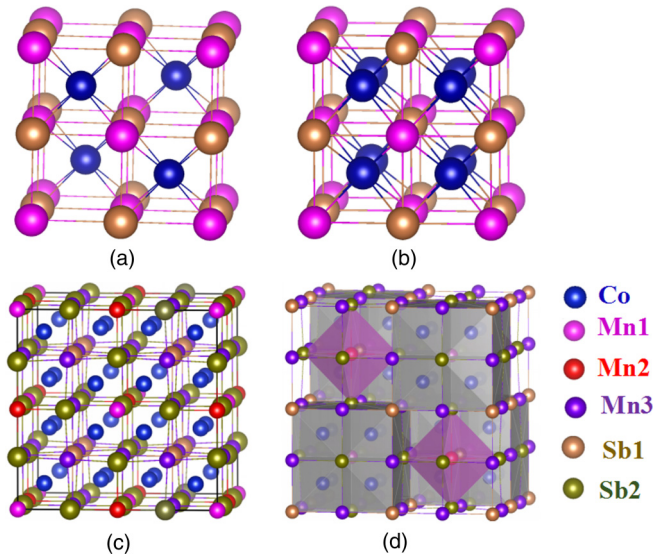*Corresponding author: g.madhu.baral@gmail.com

FIG. 1. Unit cell of (a) CoMnSb in $C1_b$ structure, (b) Co$_2$MnSb in $L2_1$ structure, and (c) CoMnSb in superstructure. (d) Alternate arrangement of Co$_2$MnSb and MnSb substructural units in the superstructure. To identify the inequivalent atoms in different sites of the unit cells, the atoms are marked with different colors.

the evolution of crystal structure and physical properties as a function of the Co content, to ascertain the potential of this system for technological applications.

As stated above, the available reports on CoMnSb and Co$_2$MnSb alloys do not provide a consistent picture of their crystal structure and magnetic properties. CoMnSb has been synthesized in bulk [24–27] and thin-film forms [21,22] by many researchers. In some of the earlier studies [24–27], although CoMnSb was reported to be synthesized in a single-phase $C1_b$ structure with the lattice parameter in the range of 5.83–5.88 Å, the measured magnetic moment was found to be in the range from 3.7 to 4.0 μ_B/f.u. These values differ considerably from the calculated value of 3 μ_B/f.u. for the $C1_b$ structure. However, the reason behind this discrepancy is not explicitly discussed in the literature. Later, Ksenofontov *et al.* [17] revisited the crystal structure by doing synchrotron-based powder x-ray diffraction (XRD) measurements and found that CoMnSb exhibits superstructure ordering in Fm-$3m$ symmetry with a lattice parameter of 11.735 Å. These conclusions are different from the study with the Fd-$3m$ space group previously reported by Senateur *et al.* [28]. In the CoMnSb superstructure with the Fm-$3m$ space group [shown in Fig. 1(c)], Co atoms occupy the set of $32f(y, y, y)$ sites with $y = 0.1221(3)$, whereas the three inequivalent Mn atoms Mn1, Mn2, and Mn3 are located at the $4a(0, 0, 0)$, $4b(0.5, 0.5, 0.5)$, and $24d(0, 0.25, 0.25)$ sites, respectively. Moreover, the two inequivalent Sb atoms Sb1 and Sb2 are located at $8c(0.25, 0.25, 0.25)$ and $24e(z, 0, 0)$ sites, respectively, with $z = 0.7394(2)$. Hence, the unit cell can be visualized as an alternate arrangement of Co$_2$MnSb and MnSb substructural units [shown in Fig. 1(d)], where the Sb1 atoms are present at the corners, Sb2 atoms are approximately at the face center, and Mn3 atoms are at the middle of the edge length of both the Co$_2$MnSb and MnSb substructural

units. The center of Co$_2$MnSb and MnSb substructural unit cells are occupied by Mn1 and Mn2 atoms, respectively. Using density-functional theory (DFT) calculations performed with the experimental lattice parameter of 11.735 Å, Ksenofontov *et al.* found a magnetic moment $\sim$4 μ_B/f.u., which is slightly higher than the measured magnetization value of 3.8 μ_B/f.u. Their calculated density of states (DOS) exhibit a metallic character for the CoMnSb superstructure. The metallic behavior of the CoMnSb superstructure has also been confirmed by the resistivity measurements reported by Xiong *et al.* [18]. Subsequently, similar type of superstructure ordering was reported by Lobov *et al.* [19] and Nakamura *et al.* [20] in the bulk CoMnSb system, and by Meinert *et al.* in the magnetron-sputtered thin films of Co-Mn-Sb [21,22]. In literature, the evidence of superstructure is also reported by Xiong *et al.* in the $X_9Y_7Z_8$ ($X =$ Fe, Ru, Co, Rh, or Ir; $Y =$ Zn; $Z =$ Sn or Sb) [29] and $X_8Y_8Z_8[X =$ Co; $Y =$ Mn (Zn); $Z =$ Sb] [18] systems, where the crystal symmetry is Fm-$3m$. Generally superstructure can be obtained in various ways, such as ordering of the vacancies present in the unit cell, position interchange of the atoms with other atoms or vacancies, substitution of a set of different atoms by a set of like atoms, etc. In CoMnSb Heusler alloy [17], the superstructure is mostly created by the ordering of the vacancies present in the unit cell. However, in half-Heusler alloy family $X_9Y_7Z_8$ ($X =$ Fe, Ru, Co, Rh, or Ir; $Y =$ Zn; $Z =$ Sn or Sb) [10,29], the superstructure ordering arises primarily due to the substitution of the Y atom with X atoms. From the studies mentioned above, the lattice parameter of the CoMnSb superstructure is found to be in the range from 11.726 to 11.835 Å and the saturation magnetization is $\sim$4 μ_B/f.u. However, from our recent DFT calculations [30], we predict half metallicity in the optimized CoMnSb superstructure, which exhibits a smaller lattice parameter (11.569 Å) and total magnetic moment (3.75 μ_B/f.u. = 30 μ_B/primitive cell). In the optimized structure, since the E_f is situated at the bottom of the HM gap of width $\sim$0.22 eV, a slightly increased experimental lattice parameter possibly results in shifting of the E_f into the valence band, thus destroying the half metallicity. Therefore, a thorough investigation is required to understand the reason behind the increased lattice parameter and the loss of half metallicity in the case of the experimental crystal structure.

Similarly, the full-Heusler alloy Co$_2$MnSb has been reported to be synthesized in bulk [23,31,32] and thin-film forms [33,34] by some researchers. However, in the literature, there is a debate on the actual composition of the sample. Although Yablonskikh *et al.* [31] have claimed their Co$_2$MnSb sample to be of single phase, they neither discuss about the actual composition of the sample nor provide a detailed structural analysis. Paudel *et al.* [32] performed XRD measurements on Co$_2$MnSb using Cu K$_\alpha$ source. Without doing structure refinement and composition analysis, the authors indexed the main XRD peaks to the $L2_1$ structure and small peaks to the impurity phase of MnSb. In both the studies, however, the measured saturation moment is found to be 5.09 μ_B/f.u., which is far below the predicted value of 6 μ_B/f.u. in the $L2_1$ structure of Co$_2$MnSb. On the contrary, Webster [23] has shown from XRD and neutron diffraction measurements that arc-melted Co$_2$MnSb does not form

in single phase. It contains two phases with compositions $Co_{1.5}MnSb$ and Co. The $Co_{1.5}MnSb$ phase is crystallized in the incompletely filled $L2_1$ structure with a lattice parameter of 5.929 Å and the balance Co has a fcc structure with a lattice parameter of 3.552 Å. Using a combination of neutron diffraction and magnetization measurements, they concluded that the magnetic moment of $Co_{1.5}MnSb$ is 4.9 μ_B (with moments of 0.75 μ_B on the Co atom and 3.76 μ_B on the Mn atom) and the magnetic moment of the Co atom in the fcc phase is 1.716 μ_B per atom. Thus, the reported information on the phase formation of this composition remains contradictory and calls for a thorough investigation.

The present work principally aims at addressing three major points: (a) the progressive evolution of the structural, magnetic, and electronic properties of the $Co_{1+x}MnSb$ system as a function of x, (b) the actual existence of the stoichiometric Co_2MnSb composition in the samples synthesized in the laboratory, and (c) the reason behind the larger experimental lattice parameter as compared to the predictions and the loss of half metallicity in the CoMnSb superstructure. We find that all the $Co_{1+x}MnSb$ samples crystallize in the superstructure phase (with the Fm-$3m$ space group) and are ferromagnetic at room temperature (RT) with a saturation magnetic moment $>4\,\mu_B$/f.u. In these samples, the additional Co atoms are accommodated in the second set of $32f\,(y', y', y')$ sites, which is otherwise vacant in the CoMnSb superstructure. However, the maximum Co that is accommodated in the vacant set of $32f$ sites is only $x = \sim 0.45$. Thus, the theoretically predicted Co_2MnSb in $L2_1$ phase does not stabilize in the bulk polycrystalline form. Minor deviation from stoichiometry in CoMnSb, i.e., excess Co and Sb as compared to Mn is accommodated in the vacant $32f$ sites of the superstructure. This explains the increase of lattice parameter and saturation magnetic moment, as compared to the calculated stoichiometric CoMnSb superstructure. Our calculations indicate that this minor deviation of stoichiometry destroys the half metallicity in the CoMnSb superstructure.

The remaining sections of the paper are organized in the following manner. Section II outlines the experimental and computational techniques. Our main results are presented in Sec. III, which consists of three subsections. These are Sec. III A: structural characterization; Sec. III B: magnetic properties, and Sec. III C: electronic structure calculations. In Sec. III A, we discuss the (A1) synchrotron XRD, (A2) optical microscopy, and scanning electron microscopy and (A3) Rietveld refinement results. In Sec. III B we analyze the measured magnetic properties and in Sec. III C, discuss the DFT results. Section IV contains concluding remarks.

II. EXPERIMENTAL AND COMPUTATIONAL TECHNIQUES

Polycrystalline samples of $Co_{1+x}MnSb$ with nominal compositions ($x = 0$, 0.25, 0.5, 0.75 and 1) were synthesized using arc-melting technique in pure (99.999%) argon atmosphere. The samples were annealed in evacuated quartz ampoules at 850 °C for 100 h, followed by natural cooling in furnace to RT. Energy-dispersive spectroscopy (EDS) measurements were performed using Bruker XFlash SDD detector in Philips XL30CP scanning electron microscope

to find out the bulk composition of the samples. Optical microscopy measurements were performed using a metallurgical microscope of make Radical Scientific Equipment and model RXLr-4. The optical microscopy, scanning electron microscopy (SEM), and EDS elemental mapping images were analyzed to understand the sample homogeneity and to identify any element segregation. Room-temperature powder XRD measurements of the annealed samples were done at the Extreme Conditions XRD beamline (BL-11) of Indus-2 synchrotron source using an x-ray beam of energy 19.7 keV. Rietveld analysis of the synchrotron XRD patterns was done using the FULLPROF software [35,36]. Magnetization (M) vs field (H) measurements (at 2 K and 300 K) were performed using a superconducting quantum interference device based vibrating sample magnetometer (MPMS-3 SQUID VSM, Quantum Design). Electronic structure calculations based on DFT [37,38] were employed to study the magnetic and electronic properties of the $2 \times 2 \times 2$ superstructure phase of Co-Mn-Sb, as implemented in the Vienna *Ab initio* Simulation Package (VASP) code [39–41]. Together with pseudopotentials for valence electrons, a plane-wave basis set was used with generalized gradient approximation (GGA) exchange-correlation functional according to the projector augmented-wave Perdew-Burke-Ernzerhof method [42–44]. To ensure the self-consistent convergence for the superstructure, the kinetic energy cutoff for plane wave expansion was taken as 500 eV and $7 \times 7 \times 7$ k-points were considered for sampling the Brillouin zone. All the calculations converge with the energy and force tolerance criterion of 10^{-6}eV and 0.01 eV/Å, respectively. A k−point sampling of $8 \times 8 \times 8$ was set in the Brillouin-zone integrations based on the Monkhorst-Pack scheme for the electronic structure (DOS) calculations [45]. The unit cells of CoMnSb in the superstructure phases have been plotted using the VESTA software [46].

III. RESULTS AND DISCUSSION

A. Structural characterization

Table I exhibits the details of the samples studied in this work. In the table, the samples with nominal composition $Co_{1+x}MnSb$ with $x = 0$, 0.25, 0.5, 0.75, and 1 have been named as CMS-1, CMS-2, CMS-3, CMS-4, and CMS-5, respectively.

1. Synchrotron x-ray diffraction results

The synchrotron XRD patterns of the samples CMS-1 to CMS-5 are shown in Fig. 2(a). The diffraction patterns of all the samples indicate superstructure ordering, as reported for CoMnSb [17–20]. For the sample CMS-5, the superstructure ordering observed in the present work is in contradiction with the $L2_1$ structure reported earlier [23,31,32]. It may be noted that for the other compositions (CMS-2, CMS-3, and CMS-4), no results are available in the literature for comparison. Moreover, to see the effect of annealing on the crystal structure, the samples were also annealed at 600 °C. It has been observed that both the as-cast and the annealed samples exhibit superstructure ordering, with only a slight variation in the lattice parameter and microstructure (see XRD patterns in Fig. S1 of Supplemental Material [47]). In this work we only discuss

TABLE I. The nominal compositions (first column) and the bulk compositions of the samples obtained from EDS measurements (second column) are presented along with the nomenclature used for the samples. The weighted-average compositions of the main Co-Mn-Sb phase, as obtained from Rietveld refinement of the XRD patterns, are shown in the third column. The saturation magnetization (M_s) values of the samples extracted from the M vs H curves at 2 K and 70 kOe are shown in the fourth column. Here, the error bar in the value of magnetization in emu/g is due to the uncertainties in the measurement of the sample mass. The corrected M_s values obtained after subtracting the magnetic contribution of 2% fcc Co (i.e., 3.25 emu/g) are presented in the fifth column. The corrected M_s values in emu/g are converted into μ_B/f.u. by using the weighted-average composition of the main Co-Mn-Sb phase (sixth column).

Nominal composition	EDS composition	XRD composition	Total value of M_s(emu/g)	Corrected value of M_s(emu/g)	Corrected value of M_s(μ_B/f.u.)
CoMnSb (CMS-1)	$Co_{1.01}Mn_{0.97}Sb_{1.02}$	$Co_{1.02}MnSb_{1.02}$	96.2 ($\pm$1.0)	96.2	4.08
$Co_{1.25}MnSb$(CMS-2)	$Co_{1.26}Mn_{0.94}Sb_{1.05}$	$Co_{1.21}MnSb$	93.1 ($\pm$1.3)	93.1	4.13
$Co_{1.5}MnSb$(CMS-3)	$Co_{1.59}Mn_{0.94}Sb_{0.98}$	$Co_{1.44}MnSb$	93.2 ($\pm$1.2)	90.0	4.22
$Co_{1.75}MnSb$(CMS-4)	$Co_{1.76}Mn_{0.97}Sb_{1.02}$	$Co_{1.46}MnSb$	94.9 ($\pm$0.9)	91.7	4.32
Co_2MnSb (CMS-5)	$Co_{1.89}Mn_{0.99}Sb_{1.12}$	$Co_{1.45}MnSb$	95.2 ($\pm$0.8)	92.0	4.32

the samples annealed at 850 °C. Figure 2(a) indicates that for the Co compositions up to $x = 0.25$, the samples (CMS-1 and CMS-2) form single-phase superstructure. Beyond this composition, the extra peaks marked by # in the XRD patterns of the samples CMS-3 to CMS-5 [see Fig. 2(a) and its inset] correspond to the fcc phase of elemental Co. Thus, some amount of Co is insoluble in the main Co-Mn-Sb phase for $x > 0.25$ and it precipitates out of the matrix as a secondary phase in these compositions. To understand the nature and location of the segregated Co, a study of the morphology of all the samples has been performed using optical microscopy, SEM, and EDS-elemental mapping.

2. Optical microscopy and scanning electron microscopy results

The samples were polished with abrasive papers of various grit sizes and finally 1-μm diamond paste was used to obtain mirror finish. The as-polished specimens were examined using an optical microscope to study the microstructural features. The optical images of the samples CMS-1 to CMS-5

are shown in Figs. 3(a)–3(e), respectively. In CMS-1, the signature of (large and continuous) grain boundaries are clearly seen. In the optical images of the other four samples (CMS-2 to CMS-5), apart from the signature of the grain boundaries, alignments of dots are also visible. These dotted lines form a spatial network over the entire sample. In several places the dotted lines form closed loops, while they form open-ended networks in many other locations. These dots seem to be etch pits, and the alignment of etch pits generally signifies the presence of dislocations [48]. As indicated by Fig. 3(a), the dislocation density in the CMS-1 sample seems to be insignificant. This figure also shows the presence of several random large black spots in CMS-1. The samples CMS-2 to CMS-5, on the other hand, reveal the presence of a different kind of black spots, which are much smaller in size and are arranged mostly along the grain boundaries. The same as-polished samples CMS-1 to CMS-5 were further studied using SEM and EDS measurements to check the sample homogeneity, to identify the segregation of elements, and to determine the actual bulk composition. Except CMS-5, the
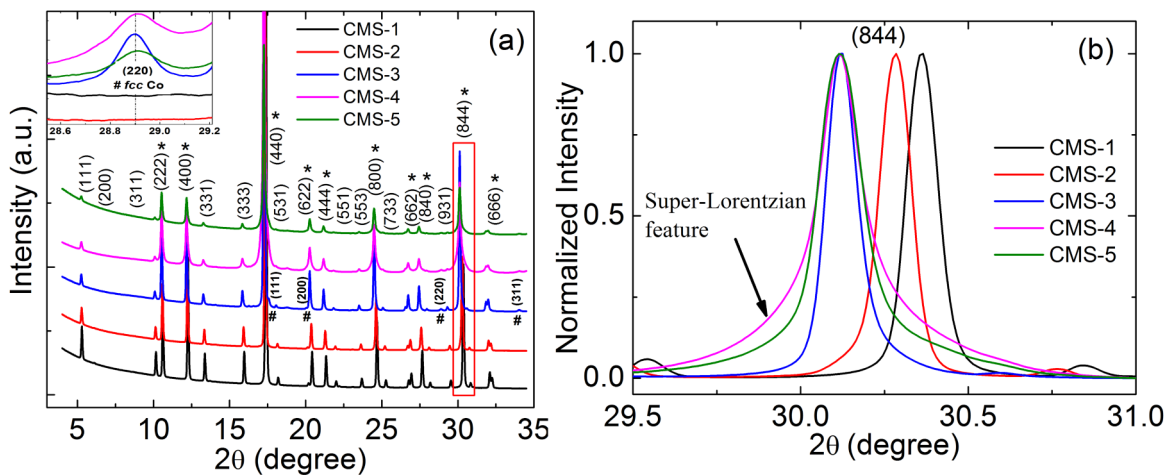

FIG. 2. (a) Room-temperature powder XRD patterns of the CMS-1 to CMS-5 samples, annealed at 850 °C. The presence of all the diffraction peaks indicates superstructure ordering. If the samples had formed in $C1_b$ or $L2_1$ structure, only the peaks marked with star (*) would have appeared in the diffraction pattern. The peak positions marked with (#) correspond to the fcc Co phase. To clearly indicate the existence of the fcc Co in the XRD profiles of the samples CMS-3, CMS-4, and CMS-5, the (220) peak is expanded and shown in the inset. (b) The normalized intensity of the (844) peak showing the change of peak shape and 2θ shift as a function of sample composition.
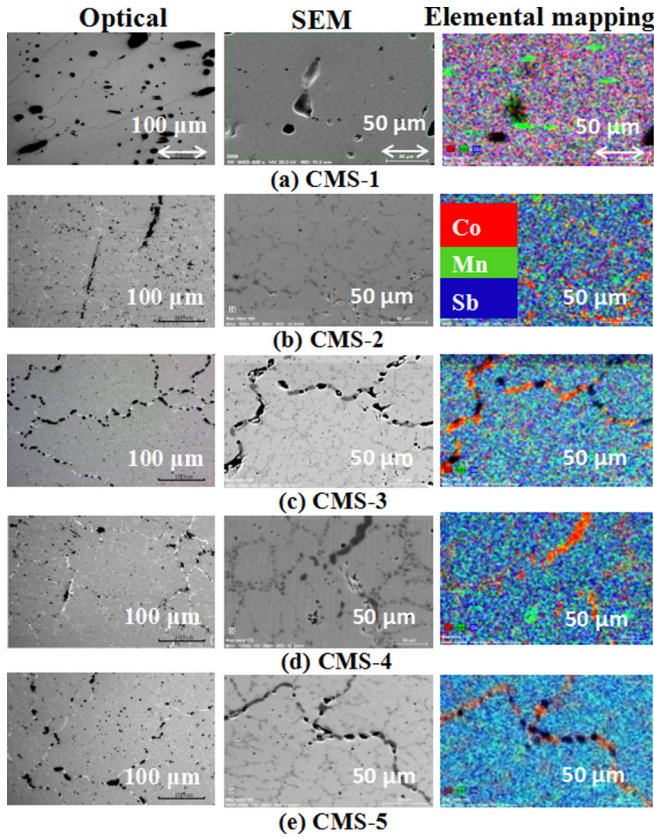
FIG. 3. Optical microscopy images (left column), SEM images (center column), and elemental mapping images (right column) of the (a) CMS-1, (b) CMS-2, (c) CMS-3, (d) CMS-4, and (e) CMS-5 samples. In elemental mapping, the red, green, and blue colors represent Co, Mn, and Sb atoms, respectively.

actual bulk EDS compositions of all the samples are found to be close to the nominal composition within the experimental accuracy (shown in Table I). The SEM images and the EDS elemental mapping images of the samples CMS-1 to CMS-5 are also shown in Figs. 3(a) to 3(e), respectively. From the figures, it is observed that all the samples are grossly uniform in composition, with some randomly scattered small-sized manganese-rich regions. Except in CMS-1, cobalt is observed to have precipitated along the grain boundaries in all the samples, though the amount is quite small in CMS-2. The SEM images reveal that the black spots of Fig. 3(a) are large holes, indicating the porous nature of this sample. In Figs. 3(b)–3(d), holes are also visible along the grain boundaries in the samples CMS-2 to CMS-5. These are probably due to the chunks of cobalt removed during sample polishing.

3. Rietveld refinement results

Rietveld refinement of the synchrotron XRD patterns was done to find the complete details of the crystal structure of the samples [35,36]. The main aim was to determine the crystallographic sites occupied by Co atoms and the percentage of Co inside the superstructure, as a function of the Co concentration in the different alloy compositions. During the refinement process, the lattice parameters, atomic coordinates (of Co and Sb2 atoms, at $32f$ and $24e$ sites, respectively),

peak shape parameters, peak asymmetry parameters, atomic displacement parameters, and site occupancy factors have been varied. Additionally, Thompson-Cox-Hastings pseudo-Voigt peak profile function was used for refinement [49,50]. For Rietveld analysis of the CMS-1 sample, the initial structural parameters were taken from the model of the CoMnSb superstructure reported by Ksenofontov *et al.* [17], which is briefly described in the Introduction. For the stoichiometric composition, the Co atoms fully occupy the set of crystallographic sites with Wyckoff position $32f(y, y, y)$, whereas the other set of $32f(y', y', y')$ sites is vacant. In the case of the off-stoichiometric compositions ($x > 0$), the extra added Co atoms partially fill the vacant $32f(y', y', y')$ sites. Here, the two Co atoms occupying the set of $32f(y, y, y)$ and $32f(y', y', y')$ crystallographic sites are labeled as Co1 and Co2, respectively, and the corresponding refined values of y and y' are given in Table II for all the samples.

For the CMS-1 sample, the fractional occupancy of the Co, Mn, and Sb atoms was refined, where the respective crystallographic sites were found to be fully occupied, i.e., Co:Mn:Sb = 1:1:1. The unit-cell parameter obtained after refinement is $a = 11.7676(2)$ Å. The observed cell parameter is slightly higher (by $\sim$0.3%) than the values previously reported by Ksenofontov *et al.* [17] and Xiong *et al.* [18]. The y and z values of the fractional coordinates of Co1(y, y, y) and Sb2($z, 0, 0$) are found to be 0.1211(1) and 0.7390(1), respectively (given in Table II). From Fig. 4(a), although the fitting quality is found to be reasonable, there is a small mismatch between the observed and calculated profiles for some of the diffraction peaks [see peak (440) in the inset]. We have tried several structural/geometrical possibilities for the refinement as discussed below. The best fit is obtained when a very small fraction of Co and Sb is considered to occupy the second, otherwise empty, set of $32f(y', y', y')$ sites (which is consistent with the elemental composition $Co_{1.01}Mn_{0.97}Sb_{1.02}$ obtained from EDS). The refined XRD pattern is shown in Fig. 4(b) and the refined parameters are shown in Table II. From the XRD measurement of CoMnSb single crystal, Nakamura *et al.* have reported a mixture of superstructure and $C1_b$ structure where the lattice constant of superstructure ($a = 11.835$ Å) is approximately two times larger than the $C1_b$ structure ($a = 5.875$ Å) [20]. In our study of the polycrystalline CMS-1 sample, the existence of half-Heusler $C1_b$ phase was not observed within the detection limit of our XRD setup. This was also confirmed by doing two-phase Rietveld refinement of the XRD pattern of the CMS-1 sample (not shown here), where a significantly poorer fit was obtained.

The Rietveld refinement of the CMS-2 alloy indicates that the first set of $32f(y, y, y)$ sites is fully occupied by the Co1 atoms, whereas the fractional occupancy of Co2 in the second set of $32f(y', y', y')$ sites is 0.207(3). The refined XRD data is shown in Fig. 4(c) and the parameters are given in Table II. The chemical composition of the Co-Mn-Sb phase in the sample, obtained after refinement of the XRD pattern, was found to be $Co_{1.21}MnSb$, which is slightly lower ($\sim$4%) than the bulk elemental composition ($Co_{1.26}Mn_{0.94}Sb_{1.05}$) obtained from the EDS measurements. This loss of Co from the main phase is consistent with the presence of segregated Co in the sample [shown in the EDS elemental mapping image in Fig. 3(b)]. Since there is no detectable XRD peak related to

TABLE II. Parameters obtained using Rietveld refinement, fractional occupancy of the Co2 and Sb3 atoms, and χ^2 values for the CMS-1, CMS-2, CMS-3, CMS-4, and CMS-5 samples. The fractional occupancy of the Co1(1.000), Mn1(0.125), Mn2(0.125), Mn3(0.750), Sb1(0.250), and Sb2(0.750) atoms in the respective crystallographic sites is 100% (not explicitly shown in the table). Fractional coordinate of the segregated Co atoms in the fcc phase (with Fm-$3m$ space group) is $4a(0, 0, 0)$. Phase 1 and phase 2 refer to the two Co-Mn-Sb phases in the samples with different structural parameters.

Sample	a(Å)	y (Co1)	y' (Co2/Sb3)	z(Sb2)	Occupancy (Co2/Sb3)	Weight%	χ^2
CMS-1	11.7676(2)	0.1211(1)		0.7391(1)		100	0.48
CMS-1	11.7672(2)	0.1209(1)	0.3661(24)	0.7387(1)	0.019(1)	100	0.27
CMS-2	11.8017(2)	0.1214(3)	0.3691(12)	0.7393(1)	0.207(3)	100	0.33
CMS-3							
Phase 1	11.8710(1)	0.1232(5)	0.3711(13)	0.7425(2)	0.479(32)	83.0(0.7)	0.25
Phase 2	11.8236(1)	0.1219(18)	0.3667(59)	0.7382(6)	0.292(19)	15.3(0.5)	
fcc Co	3.5673(2)					1.7(0.3)	
CMS-4							
Phase 1	11.8710(1)	0.1232(5)	0.3711(13)	0.7425(2)	0.469(14)	50.1(0.3)	0.90
Phase 2	11.8462(2)	0.1227(10)	0.3715(11)	0.7424(1)	0.468(9)	48.4(0.3)	
fcc Co	3.5619(4)					1.5(0.5)	
CMS-5							
Phase 1	11.8670(2)	0.1236(2)	0.3712(15)	0.7430(2)	0.462(9)	55.5(0.7)	0.16
Phase 2	11.8367(7)	0.1232(2)	0.3710(10)	0.7421(4)	0.447(17)	43.2(0.8)	
fcc Co	3.5619(1)					1.3(0.7)	

either hcp or fcc Co, this precipitated Co at the grain boundaries may be either in an amorphous/nanocrystalline form or the percentage of the crystalline Co is so small that it is below the experimental detection limit..

For the sample CMS-3, the XRD peaks are asymmetric towards higher 2θ value. Additionally, there are some small diffraction peaks corresponding to the fcc Co structure in the XRD pattern [marked with # in Fig. 2(a) and in its inset]. Three-phase Rietveld refinement was performed to understand the XRD pattern in full details. Phase 1 and phase 2 correspond to the two Co-Mn-Sb phases with different compositions and lattice parameters, whereas the third phase is taken as fcc Co. The refined pattern is shown in Fig. 4(d) and the parameters are presented in Table II. After refinement, the weight percentages of the phase 1, phase 2, and fcc Co were found to be ∼83, ∼15.3, and ∼1.7%, respectively. This finding is consistent with the Co segregation observed in the grain boundaries [shown in the EDS elemental mapping image in Fig. 3(c)]. The weighted-average value of the fractional occupancy of Co2 in the second set of $32f(y', y', y')$ sites is estimated to be 0.441(2). In this sample, although ∼12% of the Co is lost from the main Co-Mn-Sb phase, only ∼1.7% is detected in the Rietveld refinement as fcc Co. The remaining precipitated Co, which is undetected in the XRD measurements, may be distributed as ultrafine particles or in a noncrystalline form.

For compositions $x > 0.5$, the XRD peaks are super-Lorentzian in nature, where the peak is sharp at the top but significantly broader towards the base as compared to the shape of a pure Lorentzian peak [51]. These profile features arise primarily due to microstructural inhomogeneities [52–56] and/or compositional gradients [55,56] in the sample. Generally, it is not possible to model such peak shapes using a single-phase Rietveld refinement that is based on pseudo-Voigt profile approximation. Therefore, a two-phase (phase 1 and phase 2) refinement was considered for the quantification of microstructural and compositional heterogeneities, as has

been reported in the literature [57,58]. Additionally, a third phase was also considered in the refinement in order to account for the fcc Co present in these samples. The multiphase Rietveld refinement of the XRD patterns of CMS-4 and CMS-5 are shown in Figs. 4(e) and 4(f), respectively. The refined parameters are presented in Table II. It was observed that the samples CMS-4 and CMS-5 consist of two Co-Mn-Sb phases with slightly different compositions. The weighted-average compositions of CMS-4 and CMS-5 are $Co_{1.462}MnSb$ and $Co_{1.449}MnSb$, respectively. The refined value of weight % of fcc Co was found to be ∼1.5% for CMS-4 and ∼1.3% for CMS-5.

From the refinement parameters of the synchrotron XRD data (given in Table II), we find that the maximum Co atomic fraction that is accommodated in the vacant $32f$ site is $x = \sim0.45$. The extra Co atoms which do not occupy the lattice site segregate out of the main phase and precipitate at the grain boundary. Moreover, out of the total segregated Co, only up to a maximum value of ∼2% is detected in the fcc phase from the synchrotron XRD measurement. The unit-cell parameter increases monotonically with increasing Co content up to ∼$x = 0.45$ (i.e., the lattice parameter increases from CMS-1 to CMS-3, and it remains nearly constant for CMS-4 and CMS-5). From the refinement results, we also observe that the y, y', and z values of the fractional coordinates of Co1(y,y,y), Co2(y', y', y'), and Sb2$(z, 0, 0)$ atoms increase with increase in Co concentration. For the subsequent analysis, we use the weighted-average XRD composition of the main Co-Mn-Sb phase of the samples.

B. Magnetic properties

Figures 5(a) and 5(b) show the M vs H curves at 2 and 300 K, respectively. All the samples are observed to be ferromagnetic even at room temperature. The values of saturation magnetization (M_s) extracted from the M vs H curve at 2 K are presented in Table I. For CMS-1, the value of M_s at 2 K
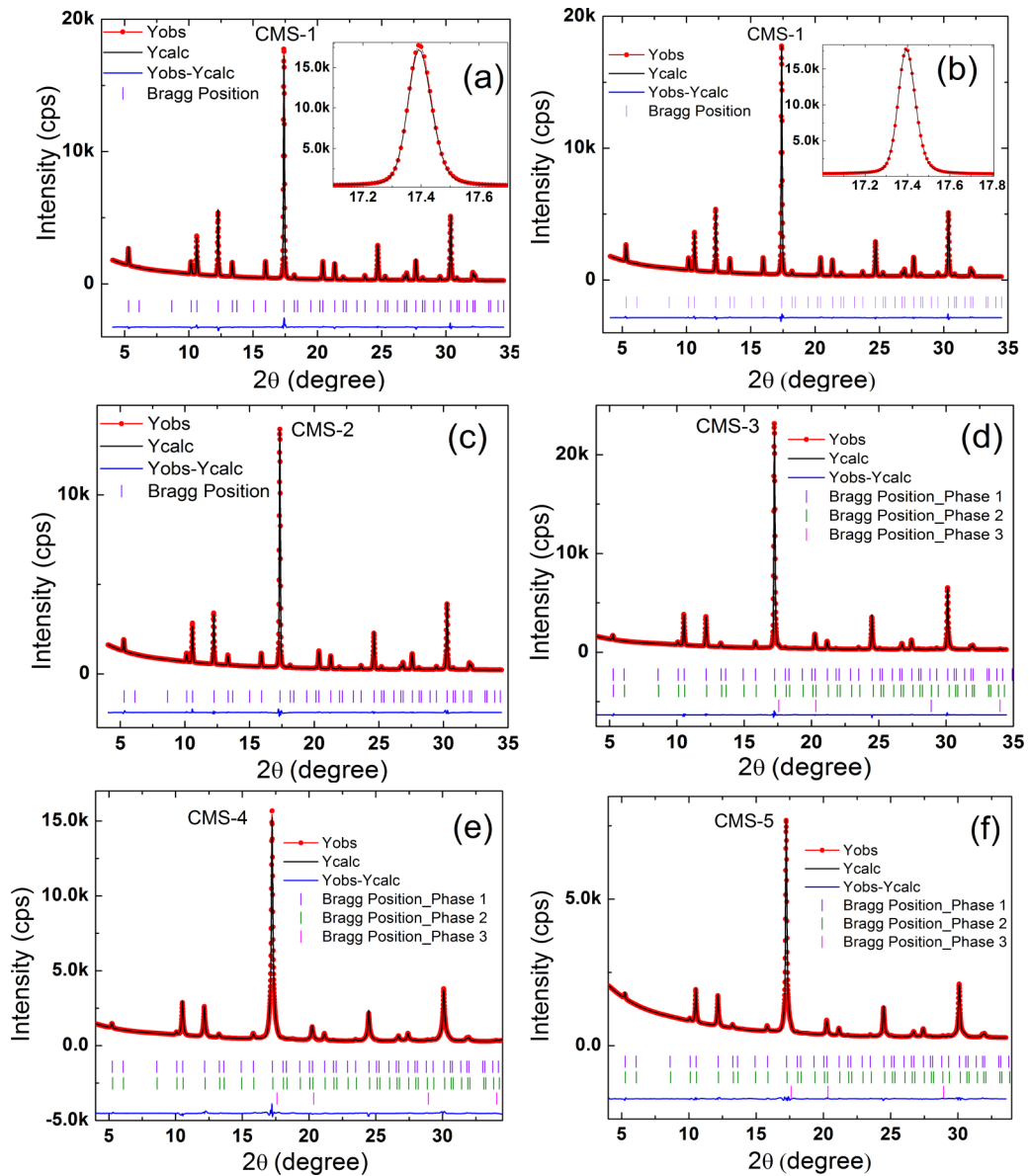
FIG. 4. Rietveld refinement of synchrotron XRD patterns for the samples (a), (b) CMS-1, (c) CMS-2, (d) CMS-3, (e) CMS-4, and (f) CMS-5, respectively. In the insets to the figures (a) and (b), the (440) peak is magnified to show the quality of fitting.
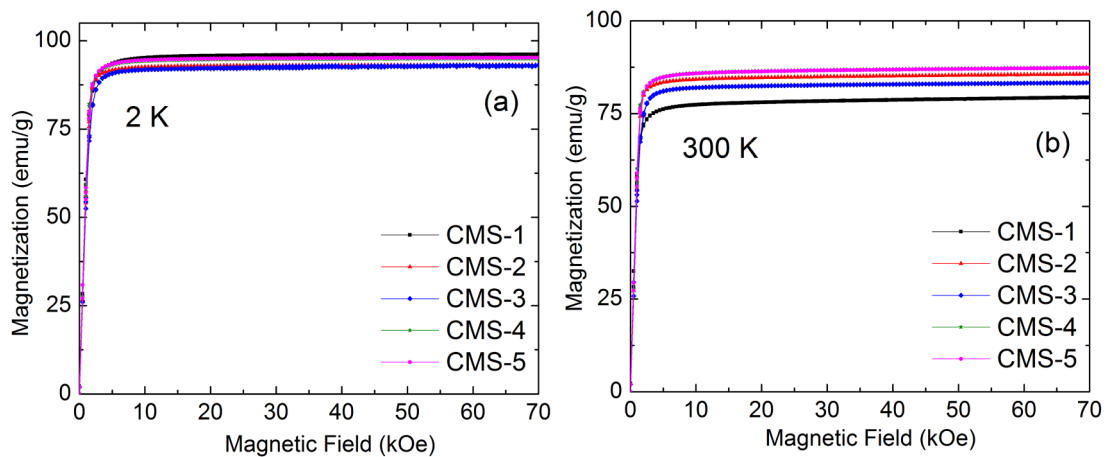

FIG. 5. M vs H curves at (a) 2 K and (b) 300 K for fields up to 70 kOe.

TABLE III. Calculated total moment and partial moments of the Co, Mn1, Mn2, Mn3, Sb1, and Sb2 atoms for different compositions. The lattice parameters used for the calculations are also shown.

Composition	Lattice parameter (Å)	$M_T(\mu_B/\text{f.u.})$	Partial magnetic moment (μ_B/atom)					
			M_{Co}	M_{Mn1}	M_{Mn2}	M_{Mn3}	M_{Sb1}	M_{Sb2}
CoMnSb	11.76757	4.03	0.52	2.73	3.14	3.55	−0.08	−0.07
$Co_{1.22}Mn_1Sb_1$	11.80173	4.31	0.68	2.82	3.21	3.46	−0.07	−0.07
$Co_{1.25}Mn_1Sb_1$	11.80173	4.29	0.67	2.82	3.22	3.44	−0.07	−0.07
$Co_{1.28}Mn_1Sb_1$	11.82429	4.37	0.70	2.87	3.28	3.44	−0.06	−0.06
$Co_{1.44}Mn_1Sb_1$	11.86395	4.62	0.82	2.96	3.34	3.39	−0.06	−0.06
$Co_{1.5}Mn_1Sb_1$	11.86395	4.80	0.90	3.02	3.34	3.38	−0.05	−0.05
$Co_{1.03}Mn_1Sb_{1.03}$[a]	11.76757	4.08	0.57	2.74	3.20	3.49	−0.07	−0.07

[a] One excess Co and Sb atom put in the second set of $32f$ sites of the CoMnSb superstructure.

is found to be 96.2 emu/g, which is the highest among all the samples. The M_s value decreases to 93.1 emu/g for the CMS-2 sample. Beyond CMS-2, the value of M_s increases to 93.2 emu/g for CMS-3, to 94.9 emu/g for CMS-4, and to 95.2 emu/g for CMS-5. But, within the error bar (shown in Table I), the value of M_s is nearly similar for all the compositions above CMS-2. From the refinement of XRD pattern, since ~2% fcc Co is found to be present as secondary phase in the samples CMS-3 to CMS-5, its magnetic contribution has been subtracted from the total M_s value of these samples. In literature [23] and from our present DFT calculations (discussed below), the magnetic moment of bulk fcc Co was found to be 1.716 μ_B/atom ($\approx$ 162.5 emu/g). Hence, a contribution of 3.25 emu/g (for 2% fcc Co) has been subtracted from the total M_s value of the samples and the corrected M_s values corresponding to the main Co-Mn-Sb phase of the samples CMS-3, CMS-4, and CMS-5 are shown in Table I. The remaining precipitated Co that remains undetected in the XRD measurements is assumed to be amorphous or nanocrystalline and do not contribute to magnetization. The corrected M_s value (in emu/g) of the main Co-Mn-Sb phase is converted to μ_B/f.u. by using the weighted-average composition obtained from the XRD measurements. These are presented in Table I. We observe that the value of M_s increases monotonically with the Co content, i.e., the M_s value actually increases from CMS-1 to CMS-4. However, for CMS-5, the value is same as CMS-4.

C. Electronic structure calculations

The synchrotron XRD and magnetization measurements show that all the $Co_{1+x}MnSb$ samples crystallize in the superstructure phase and are ferromagnetic at room temperature. Their saturation magnetic moment is >4 μ_B/f.u., which increases monotonically with increasing Co content up to a maximum for $x = \sim0.45$. To explain the observed increase in the M_s value and to get insight into the electronic structure, we have performed DFT calculations of the $Co_{1+x}MnSb$ system by using the experimental lattice parameters, atomic coordinates, and the compositions close to the weighted-average composition of the Co-Mn-Sb phase obtained from the Rietveld refinement (see Table I). To account for the off-stoichiometric composition of $Co_{1+x}MnSb$, all the calculations were performed in reduced ($P1$) symmetry with lattice parameters $a = b = c$ and angles $\alpha = \beta = \gamma = 90°$.

Moreover, in order to confirm the randomness of filling the Co atoms at the second set of $32f(y', y', y')$ sites, random numbers were generated and the atoms were arranged according to the same for the calculation. To understand the reason behind the observed difference between the experimental and calculated lattice parameters, an analysis is performed in the last part of this section.

Table III shows the calculated total spin magnetic moment per formula unit and partial spin moments of the Co, Mn1, Mn2, Mn3, Sb1, and Sb2 atoms for different compositions. For all the compositions, the magnetic moment of the Co atom is aligned ferromagnetically with the Mn1, Mn2, and Mn3 atoms. While the partial moments of Mn1 and Mn2 atoms increase with increasing Co concentration, the partial moment of Mn3 decreases simultaneously and results in a nearly constant average moment of the Mn atoms (~3.33 to ~3.39 μ_B/atom). However, the average partial moment of the Co atoms increases from 0.52 to 0.90 μ_B/atom with increasing Co concentration. Therefore, due to the simultaneous increase in the number of Co atoms and its average partial moment, there is a net enhancement of the total magnetic moment from 4.03 to 4.79 μ_B/f.u. (shown in Table III). Our calculated results are consistent with the x-ray magnetic circular dichroism results on Co-Mn-Sb thin films [21,22]. In these films, the spin magnetic moment of the Co atom increases with increasing Co concentration, whereas the Mn spin moment remains constant. Comparing with these results we find that the calculated total moment of the CoMnSb superstructure is in good agreement with the measured M_s value (shown in Table I). Moreover, our calculated total and partial moments of CoMnSb corroborate with the moments reported by Ksenofontov *et al.* [17]. For samples with higher Co contents, the experimental values of magnetization were found to be slightly smaller than the calculated moments (shown in Table III). This discrepancy seems to arise because the composition used for the calculation is not exactly the same as the actual composition of the samples obtained from XRD. Since the actual composition of CMS-1 sample (as obtained from Rietveld refinement) is slightly excess in Co and Sb, the calculation was also performed by adding one extra Co atom and Sb atom at the second set of $32f$ sites in the unit cell of the CoMnSb superstructure. It has been observed that with an increase in Co and Sb atoms at the second set of $32f$ sites, there is a marginal increase in the partial moment of the Co atom and consequently an increase in the total moment
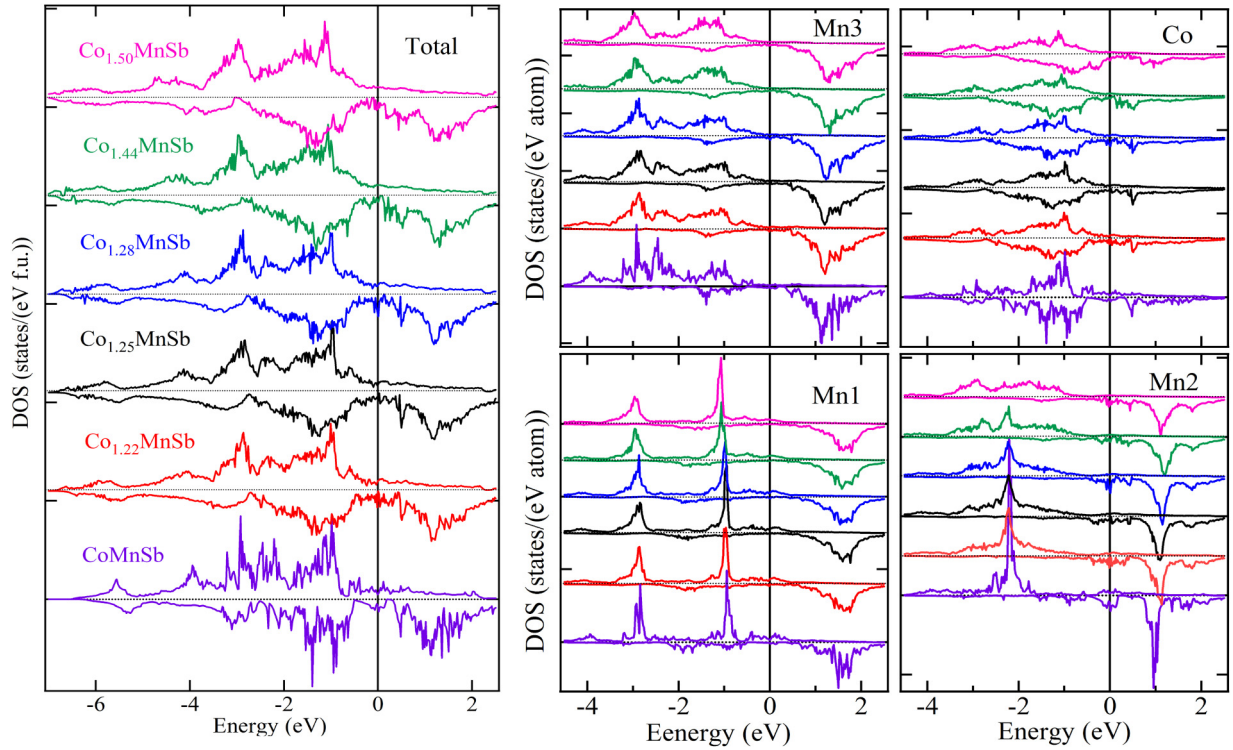
FIG. 6. Comparison of spin-polarized total DOS and partial DOS calculated for different compositions of the Co-Mn-Sb superstructure. The E_f has been set to zero.

per formula unit. Further, we find that this value of the total magnetic moment is closer to the experimental M_s for the sample CMS-1.

Figure 6 shows the comparison of spin-polarized total DOS and partial DOS of the Co, Mn1, Mn2, and Mn3 atoms for different compositions (as shown in Table III). From the total DOS, all the compositions are found to be metallic with finite up- and down-spin states at the E_f. In all the cases, the valence band is dominated by the hybridized Co and Mn 3d states. However, among all the three types of Mn atoms in the superstructure, since the degeneracy of the Mn3 (24d) is higher than Mn1 (4a) and Mn2 (4b) in the Fm-3m symmetry, the 3d states of the Mn3 atom have larger contribution in the valence band than Mn1 and Mn2 atoms. The total DOS calculated in this work for the CoMnSb superstructure matches well with the DOS reported by Ksenofontov *et al.* [17]. It has been observed that for the CoMnSb superstructure, a pseudogap is present in the down-spin channel of the conduction band, whereas for other compositions no such gap is found. From the spin-polarized DOS presented in our previous DFT calculations [30], we have seen that the E_f is situated at the bottom of the minority spin HM gap. As the experimental lattice parameter increases (11.7676 Å), the E_f moves towards higher binding energy (in the valence band) and the half-metallic gap lies in the conduction band making the material metallic (see Fig. 6). Additionally, we find from Fig. 6 that the partial DOS of three inequivalent Mn atoms are significantly different, which is due to the different near-neighbor atomic arrangement. The details of the partial DOS of the Co and Mn atoms and their correlation with the near-neighbor geometry of the CoMnSb superstructure have been presented in our

previous work [30]. In the CoMnSb superstructure, as one set of the 32f sites is vacant, the Mn2 atoms experience the octahedral crystal field created by the nearest-neighbor Sb1 and Sb2 atoms. Therefore, its partial DOS shows localized nature of the 3d states. As the Co concentration increases, the Co atoms start occupying the second set of the (vacant) 32f sites. Hence, the Mn2 atoms experience additional crystal field due to the nearest-neighbor Co atoms. However, since the crystal symmetry is different from regular tetrahedron, the 3d states of the Mn2 atom become delocalized. This simultaneous increase in the lattice parameter and deviation of symmetry with increasing Co concentration is the most probable reason behind the loss of half metallicity in the experimentally synthesized Co$_{1+x}$MnSb alloys. To further confirm our findings, we have calculated the magnetic moment and DOS of the Co$_{1+x}$MnSb system for different Co concentrations ($x = 0$, 0.125, 0.25, 0.375, and 0.5), after fully optimizing the crystal structure. We find that with increasing the Co concentration the lattice parameter as well as the magnetic moment of the optimized structure increase, and the materials become metallic. From the above observations, we conclude that the extra Co atoms which occupy the vacant set of 32$f(y', y', y')$ sites of the CoMnSb superstructure tend to expand the unit cell and result in the increase of the magnetic moment. This important result is used for explaining the increase of lattice parameter with respect to the optimized one for CoMnSb.

As discussed above, the experimental lattice parameter of the CMS-1 sample is larger (by ~1.7%) than the optimized lattice parameter of the CoMnSb superstructure calculated using GGA exchange-correlation functional [30]. Although

such a difference of lattice parameter between theory and experiment is expected, the reasons related to the stoichiometry and point defects in the sample cannot be ruled out, as these can naturally occur in samples due to the high temperature of synthesis. We now explore some of the possible reasons for the increased lattice parameter, magnetic moment, and loss of the half metallicity of the experimentally observed superstructure of CoMnSb in comparison with its optimized structure.

In our previous computational work, we have investigated the role of intrinsic defects on the properties of the ordered CoMnSb superstructure [30]. We found that certain types of atomic swapping and antisite defects result in the increase of lattice parameters and magnetic moment, although these defects lead to higher energy compared the ordered structure. For the synchrotron XRD pattern of the CMS-1 sample (the sample closest to the exact 1:1:1 stoichiometry), we performed Rietveld refinement by considering these defects in the 1:1:1 composition and found a poor-quality fit. Additionally, from the Rietveld refinement of the XRD pattern of the CMS-1 sample, we find that the quality of fit is slightly poorer when the exact 1:1:1 composition is chosen [see Fig. 4(a)]. However, the fitting quality improves when the vacant set of $32f$ sites is partially occupied by either of the Co, Mn, and Sb atoms or some combination of these elements. The refinement data are shown in Fig. S2 and Table S1 in the Supplemental Material [47]. To understand this aspect further, we have calculated the DOS and magnetic moment by putting some extra Co, Mn, and Sb atoms separately at the second set of $32f$ sites of CoMnSb superstructure and then optimized the structure. The optimized structure showed that the lattice parameter increases in all three cases (see Table S2 in the Supplemental Material [47]); however, the total magnetic moment increases only when Co and Sb atoms occupy the vacant set of $32f$ sites. Since the filling of the vacant site with Mn atoms results in the reduction of the total moment, this possibility can be ruled out. Among the other two possibilities (i.e., excess Co and Sb atoms), although the magnetic moment increases in both the cases, the lattice parameters for the Co excess case and Sb excess case are, respectively, slightly lower and higher than the experimental lattice parameter. Thus, in CMS-1, the small off-stoichiometry in the composition (i.e., excess Co and Sb atoms) is accommodated by filling the vacant set of $32f$ sites of the superstructure. It may be noted that the best fit of the refinement is also obtained in this condition [Fig. 4(b)]. From the above analysis, we conclude that the slight off-stoichiometry (higher Co and Sb concentration by about 3%, relative to the Mn concentration) in the composition of CMS-1 results in an increased lattice parameter and magnetic moment, as compared to the stoichiometric ordered CoMnSb superstructure. The results of DOS calculations also indicate that this minor deviation of stoichiometry destroys the half metallicity in CoMnSb superstructure. Thus, half metallicity can possibly be preserved in this system only in very highly controlled conditions for sample preparation.

IV. CONCLUSION

We have performed a combined experimental and theoretical study of the $Co_{1+x}MnSb$ system. We find that all the arc-melted polycrystalline samples show superstructure ordering, belonging to the Fm-$3m$ space group. In these samples, the additional Co is accommodated in the otherwise vacant set of $32f(y', y', y')$ sites in the CoMnSb superstructure. However, the maximum Co that is accommodated in the vacant sites is $x = \sim 0.45$. The excess Co atoms which do not occupy the lattice site segregate out of the main phase and precipitate at the grain boundaries. Thus, the theoretically predicted Co_2MnSb in $L2_1$ phase does not stabilize in the bulk polycrystalline form. Out of the segregated Co atoms, only $\sim 2\%$ is crystallized in the fcc phase. The remaining amount, which is not detected in the XRD measurements, probably forms an amorphous or nanocrystalline phase. For compositions with $x > 0.25$, the XRD peaks are asymmetric (for CMS-3 sample) and super-Lorentzian in nature (for CMS-4 and CMS-5 samples). These profile features arise primarily due to the microstructural inhomogeneities and/or compositional gradients in the sample. All the samples are found to be ferromagnetic well above room temperature. The saturation magnetization (M_s) at 2 K increases slightly from 4.08 to 4.31 μ_B/f.u. with increasing Co content.

DFT-based electronic structure calculations, using the structural and compositional parameters obtained from the Rietveld refinement of the synchrotron XRD patterns, show that the total magnetic moment per formula unit increases with increasing Co content, primarily due to the increase in partial moment of the Co atoms. The DOS calculated for all the compositions show metallic behavior. Finally, combining the experimental observations, Rietveld refinement of XRD patterns, and DFT calculations, we conclude that minor deviation from stoichiometry in CoMnSb, i.e., excess Co and Sb as compared to Mn, is accommodated in the vacant set of $32f$ sites of the superstructure. This explains the increase in the lattice parameter and saturation magnetic moment, as compared to the calculated stoichiometric CoMnSb superstructure. The calculations also indicate that this minor deviation of stoichiometry destroys the half metallicity in the CoMnSb superstructure.

[1] R. A. de Groot, F. M. Mueller, P. G. van Engen, and K. H. J. Buschow, Phys. Rev. Lett. **50**, 2024 (1983).

[2] C. Felser, G. H. Fecher, and B. Balke, Angew. Chem. Int. Ed. **46**, 668 (2007).

[3] M. Shaughnessy, R. Snow, L. Damewood, and C. Y. Fong, J. Nanomater. **2011**, 140805 (2011).

[4] C. J. Palmstrøm, Prog. Cryst. Growth Charact. Mater. **62**, 371 (2016).

[5] R. Farshchi and M. Ramsteiner, J. Appl. Phys. **113**, 191101 (2013).

[6] F. Casper, T. Graf, S. Chadov, B. Balke, and C. Felser, Semicond. Sci. Techno. **27**, 063001 (2012).

[7] C. Felser and B. Hillebrands, J. Phys. D: Appl. Phys. **40**, E01 (2007).

[8] I. Galanakis, P. H. Dederichs, and N. Papanikolaou, Phys. Rev. B **66**, 134428 (2002).

[9] M. Baral, S. Banik, A. Chakrabarti, D. M. Phase, and T. Ganguli, J. Alloys Compd. **645**, 112 (2015).

[10] M. Baral and A. Chakrabarti, Phys. Rev. B **99**, 205136 (2019).

[11] B. Xu and M. Zhang, J. Magn. Magn. Mater. **323**, 939 (2011).

[12] H. M. Huang, S. J. Luo, and K. L. Yao, Physica B **406**, 1368 (2011).

[13] M. V. Yablonskikh, Y. M. Yarmoshenko, I. V. Solovyev, E. Z. Kurmaev, L.-C. Duda, T. Schmitt, M. Magnuson, J. Nordgren, and A. Moewes, J. Electron. Spectrosc. Relat. Phenom. **144**, 765 (2005).

[14] F. Ak, F. Güçlü, B. Saatci, N. Kervan, S. Kervan, J. Supercond., Nov. Magn. **29**, 409 (2016).

[15] H. Lashgari, M. R. Abolhassani, A. Boochani, E. Sartipi, R. Taghavi-Mendi, and A. Ghaderi, Indian J. Phys. **90**, 909 (2016).

[16] Enamullah and S-C. Lee, J. Alloys Compd. **765**, 1055 (2018).

[17] V. Ksenofontov, G. Melnyk, M. Wojcik, S. Wurmehl, K. Kroth, S. Reimann, P. Blaha, and C. Felser, Phys. Rev. B **74**, 134426 (2006).

[18] D. B. Xiong, N. L. Okamoto, T. Waki, Y. Zhao, K. Kishida, and H. Inui, Chem. Eur. J. **18**, 2536 (2012).

[19] I. D. Lobov, A. A. Makhnev, and M. M. Kirillova, Phys. Met. Metallogr. **113**, 135 (2012).

[20] H. Nakamura, M. Y. P. Akbar, T. Tomita, A. A. Nugroho, and S. Nakatsuji, JPS Conf. Proc. **29**, 013004 (2020).

[21] M. Meinert, J.-M. Schmalhorst, D. Ebke, N-N. Liu, A. Thomas, G. Reiss, J. Kanak, T. Stobiecki, and E. Arenholz, J. Appl. Phys. **107**, 063901 (2010).

[22] J. Schmalhorst, D. Ebke, M. Meinert, A. Thomas, G. Reiss, and E. Arenholz, J. Appl. Phys. **105**, 053906 (2009).

[23] P. J. Webster, J. Phys. Chem. Solids **32**, 1221 (1971).

[24] M. J. Otto, R. A. M. van Woerden, P. J. van der Valk, J. Wijngaard, C. F. van Bruggen, C. Haas, and K. H. J. Buschow, J. Phys.: Condens. Matter **1**, 2341 (1989).

[25] N. P. Duong, L. T. Hung, T. D. Hien, N. P. Thuy, N. T. Trung, and E. Bruck, J. Magn. Magn. Mater. **311**, 605 (2007).

[26] S. Li, Z. Yuan, L. Y. Lü, M. Liu, Z. Huang, F. Zhang, and Y. Du, Mater. Sci. Eng. A **428**, 332 (2006).

[27] K. Kumar, A. Dashora, N. L. Heda, H. Sakurai, N. Tsuji, M. Itou, Y. Sakurai, and B. L. Ahuja, J. Phys.: Condens. Matter **29**, 425805 (2017).

[28] P. Senateur, A. Rouault, R. Fruchart, and D. Fruchart, J. Solid State Chem. **5**, 226 (1972).

[29] D. B. Xiong, Y. Zhao, N. L. Okamoto, C. Pietzonka, T. Waki, and H. Inui, Inorg. Chem. **49**, 10536 (2010).

[30] M. Baral, T. Ganguli, and A. Chakrabarti, Comput. Mater. Sci. **210**, 111441 (2022).

[31] M. V. Yablonskikh, Y. M. Yarmoshenko, E. G. Gerasimov, V. S. Gaviko, M. A. Korotin, E. Z. Kurmaev, S. Bartkowski, and M. Neumann, J. Magn. Magn. Mater. **256**, 396 (2003).

[32] M. R. Paudel, C. S. Wolfe, H. Patton, I. Dubenko, N. Ali, J. A. Christodoulides, and S. Stadler, J. Appl. Phys. **105**, 013716 (2009).

[33] M. R. Paudel, C. S. Wolfe, N. Ali, S. Stadler, J. A. Christodoulides, D. L. Ederer, Y. Li, T. A. Callcott, and J. W. Freeland, J. Appl. Phys. **105**, 103907 (2009).

[34] C. Guillemard, S. Petit-Watelot, L. Pasquier, D. Pierre, J. Ghanbaja, J.-C. Rojas-Sánchez, A. Bataille, J. Rault, P. Le Fèvre, F. Bertran, and S. Andrieu, Phys. Rev. Appl. **11**, 064009 (2019).

[35] H. M. Rietveld, J. Appl. Crystallogr. **2**, 65 (1969).

[36] J. Rodriguez-Carvajal, Physica B **192**, 55 (1993).

[37] P. Hohenberg and W. Kohn, Phys. Rev. **136**, B864 (1964).

[38] W. Kohn and L. Sham, Phys. Rev. **140**, A1133 (1965).

[39] G. Kresse and J. Hafner, Phys. Rev. B **49**, 14251 (1994).

[40] G. Kresse and J. Furthmüller, Phys. Rev. B **54**, 11169 (1996).

[41] M. Fuchs and M. Scheffler, Comput. Phys. Commun. **119**, 67 (1999).

[42] P. E. Blöchl, Phys. Rev. B **50**, 17953 (1994).

[43] G. Kresse and D. Joubert, Phys. Rev. B **59**, 1758 (1999).

[44] J. P. Perdew, K. Burke, and M. Ernzerhof, Phys. Rev. Lett. **77**, 3865 (1996).

[45] H. J. Monkhorst and J. D. Pack, Phys. Rev. B **13**, 5188 (1976).

[46] K. Momma and F. Izumi, J. Appl. Crystallogr. **41**, 653 (2008). http://jp-minerals.org/vesta/en.

[47] See Supplemental Material at http://link.aps.org/supplemental/10.1103/PhysRevB.105.184106 for additional information. Figure S1 shows room-temperature powder XRD patterns of the CMS-1 to CMS-5 samples in (a) as-cast and (b) annealed (600°C) conditions. (c) The normalized intensity of the (440) peak for different compositions indicates the change of peak shape and 2θ shift as a function of annealing conditions (as cast, 600 °C, and 850 °C). Rietveld refinement of the synchrotron XRD pattern of the CMS-1 sample by separately putting excess Co, Mn, and Sb atoms at the vacant $32f$ site of the superstructure is presented in Fig. S2. The corresponding refinement parameters are shown in Table S1. Table S2 gives optimized lattice parameters, calculated total moment, and partial moments of the Co, Mn1, Mn2, Mn3, Sb1, and Sb2 atoms for different compositions.

[48] Md. Matin, L. S. Sharath Chandra, M. K. Chattopadhyay, R. K. Meena, R. Kaul, M. N. Singh, A. K. Sinha, and S. B. Roy, J. Appl. Phys. **113**, 163903 (2013).

[49] P. Thompson, D. E. Cox, and J. B. Hastings, J. Appl. Crystallogr. **20**, 79 (1987).

[50] L. W. Finger, D. E. Cox, and A. P. Jephcoat, J. Appl. Crystallogr. **27**, 892 (1994).

[51] G. K. Wertheim, M. A. Butler, K. W. West, and D. N. E. Buchanan, Rev. Sci. Instrum. **45**, 1369 (1974).

[52] R. A. Young and A. Sakthivel, J. Appl. Crystallogr. **21**, 416 (1988).

[53] N. C. Popa and D. Balzar, J. Appl. Crystallogr. **35**, 338 (2002).

[54] J. I. Langford, D. Louër, and P. Scardi, J. Appl. Crystallogr. **33**, 964 (2000).

[55] A. Bhakar, P. Gupta, P. N. Rao, M. K. Swami, P. Tiwari, T. Ganguli, and S. K. Rai, J. Appl. Crystallogr. **54**, 498 (2021).

[56] V. Uvarov and I. Popov, Cryst. Eng. Commun. **17**, 8300 (2015).

[57] A. Leineweber and E. J. Mittemeijer, J. Appl. Crystallogr. **37**, 123 (2004).

[58] X. Wang, J. Li, R. G. McDonald, A. van Riessen, and R. D. Hart, J. Appl. Crystallogr. **48**, 814 (2015).